

Utah State University

DigitalCommons@USU

International Symposium on Hydraulic
Structures

May 16th, 5:40 PM

Performance Assessment of FLOW-3D and XFlow in the Numerical Modelling of Fish-bone Type Fishway Hydraulics

Su-Chin Chen

National Chung Hsing University, Taichung, scchen@nchu.edu.tw

S.S. Tfwala

samkelet@gmail.com

Follow this and additional works at: <https://digitalcommons.usu.edu/ishs>

Recommended Citation

Chen, Su-Chin (2018). Performance Assessment of FLOW-3D and XFlow in the Numerical Modelling of Fish-bone Type Fishway Hydraulics. Daniel Bung, Blake Tullis, 7th IAHR International Symposium on Hydraulic Structures, Aachen, Germany, 15-18 May. doi: 10.15142/T3HH1J (978-0-692-13277-7).

This Event is brought to you for free and open access by the Conferences and Events at DigitalCommons@USU. It has been accepted for inclusion in International Symposium on Hydraulic Structures by an authorized administrator of DigitalCommons@USU. For more information, please contact digitalcommons@usu.edu.



Performance Assessment of FLOW-3D and XFlow in the Numerical Modelling of Fish-Bone Type Fishway Hydraulics

S.C. Chen¹ & S.S. Tfwala¹

¹Department of Soil and Water Conservation, National Chung Hsing University, Taichung, Taiwan
E-mail: samkelet@gmail.com

Abstract: The advancement of computational power has afforded the resolving of more complex flows in three-dimensional space. Several numerical codes have been developed and to single out which method to use is becoming a more complicated task. In this study two Computational Fluid Dynamic (CFD) platforms, FLOW-3D and XFlow, are presented on 3D turbulent flows in a fish-bone type fishway. One of the basic yet most crucial steps in a number of CFD codes is the creation of efficient computational meshes for real world applications. Regardless of the numerical method applied, the mesh quality will have pronounced effects on the final results. Owing to these effects, mesh based (FLOW-3D) and meshless (XFlow) CFD codes are evaluated. FLOW-3D solves the Reynolds averaged Navier-Stokes equations and the continuity equation with the aid of Fractional Area-Volume Obstacle Representation (FAVOR), while XFlow is particle based fully Lagrangian based on the Lattice-Boltzmann method solver. For both codes, turbulence is treated using the Large Eddy Simulation (LES) model. Numerical model accuracy is assessed, comparing the complex flow field in the fishway with fish migration behaviour of fish-swimming species in a laboratory experiment. In addition, computational times and the performance of the models at different discharge rates (0.016 and 0.075 m³/s), classified as low and medium, respectively, are assessed. Generally, the findings indicated that FLOW-3D better estimated the flow structure, velocity distribution, and flow depth compared to XFlow, while XFlow was relatively faster in terms of computational time despite compromised accuracies.

Keywords: FLOW-3D, XFlow, fish-bone-type fishway, LES model

1. Introduction

Mesh free methods have been developed in an attempt to bypass the need of applying meshes for space discretization. In principle, these methods advocate for a different spatial discretization of the problem geometry, where the domain is discretized with a set of particles or nodes with some kind of interconnection among them but without the need of establishing such a specific connectivity as in the case of a conventional mesh. All major fields of Computational Fluid Dynamics (CFD), including Finite Difference Methods (FDM), Finite Element Methods (FEM), and Finite Volume Methods (FVM), have conventionally relied on the adoption of elements, intertwined grids, or finite volumes as the fundamental structures on which to discretize governing Partial Differential Equations (PDE). Despite their wide adoption and successful validation with extensive formulations and analyses, obtaining a suitable mesh poses great challenges for computational engineers (Prostomolotov et al. 2014). Mesh based CFD methods have been proven to have more difficulties in capturing deformation of free surfaces and interfaces (Liu et al. 2005), despite some viable solutions by Hirt and Nichols (1981) through their Volume of Fluid (VOF) and marker and cell by Harlow (1964). It is not yet apparent how effective meshless CFD will be at alleviating meshing problems, especially because even though a rigid mesh is not required, sufficiently dense point distributions are still required. Nonetheless, significant progress has been made on developing the next generation CFD models. Chen et al. (2010) proposed a highly 3D Lattice Boltzmann Model (LBM) for high speed compressible flows and was successful in modelling flows from subsonic to supersonic and jumps from shockwaves. Shakibaenia and Jin (2011) successfully developed a mesh-free particle model for simulating mobile bed dam break, adding among the most recently developed Smoothed Particle Hydrodynamics (SPH) and Moving Particle Semi-Implicit (MPS) methods. XFlow was applied by Kueh et al. (2014) to analyse numerically water vortex formations for water vortex plants and by Prostomolotov et al. (2014) to simulate hydrodynamic structures. In a comparative assessment of mesh based and meshless CFD models coupled with Discrete Element Method (DEM), Markauskas et al. (2017) modelled particle laden flows. Both models agreed well with analytical results. They were found to differ mainly in computed fluid fractions. In actual applications, selecting the most suitable numerical model when faced with fluid mechanics problems can be a daunting task given the wide range of possible choices. Bayon et al. (2016) compared 2 conventional mesh methods, FLOW-3D and the open source code OpenFOAM, in their hydraulic jump studies. FLOW-3D was found to be better at modelling supercritical and subcritical flows, while OpenFOAM better predicted the hydraulic jump. In this paper, two popular CFD platforms are compared: FLOW-3D (mesh based) and XFlow (meshless) in terms of accuracy (turbulence, flow depth, and velocity)

and processing times. A case study based on complex flow fields in a fish-bone-type fishway is simulated. For validation purposes, results are compared to data obtained from the author's published flume experiments on the hydraulics-driven upstream migration of Taiwanese indigenous fishes in a fish-bone-type fishway (Chen et al. 2017), and the reader is referred to this study for detailed experiment setup.

2. The Fishway

The fishway under study is a fish-bone-type in a laboratory flume with a length and width of 10 m and 1 m, respectively. The base is made of 0.006 m steel bed panel, while the walls consist of transparent acrylic. The slope of the flume was fixed at 1/10. This fish-bone-type fishway consisted of 3 main regions: blocks, fish-bone area, and a channel area demarcating the blocks to fish-bone area (Figure 1). Attached on the fish-bone frames were 0.1×0.1 (height and width) fish-bones at a 45° angle. Blocks ($0.756 \text{ m long} \times 0.2 \text{ m wide} \times 0.25 \text{ m high}$) were fixed along the flume walls, leaving rest areas of 0.524 m long and 0.2 m wide between the blocks.

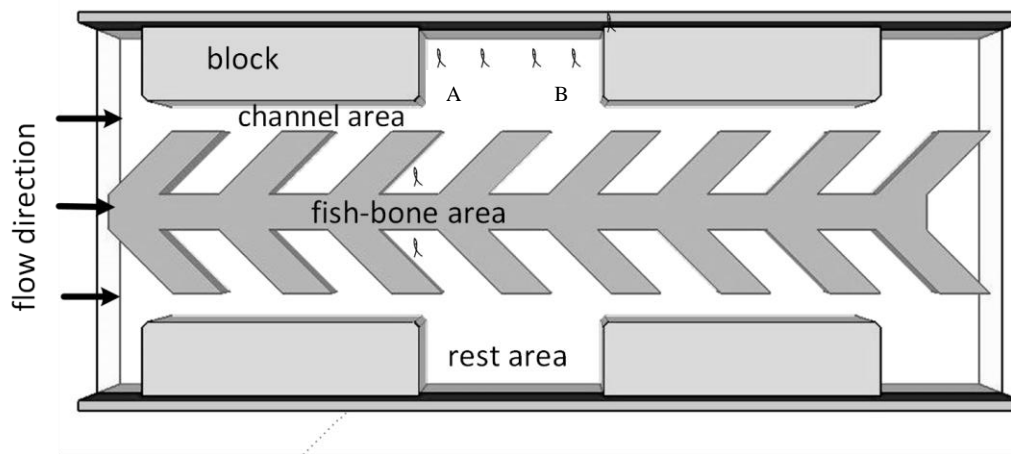


Figure 1. Three main regions in the fish-bone-type fishway.

2.1. Laboratory Data Collection

Data collected for model validation included flow velocity and flow depth. Flow velocity was measured using a 2D electromagnetic instrument, VM801D main unit, VMT2-300-04P probe, KENEK. Flow depth measurements were done through a fine-scale Vernier needle gauge installed vertically in the fishway. Measurements were conducted in all three major regions of the fish-bone-type fishway as seen in Fig. 2 below.

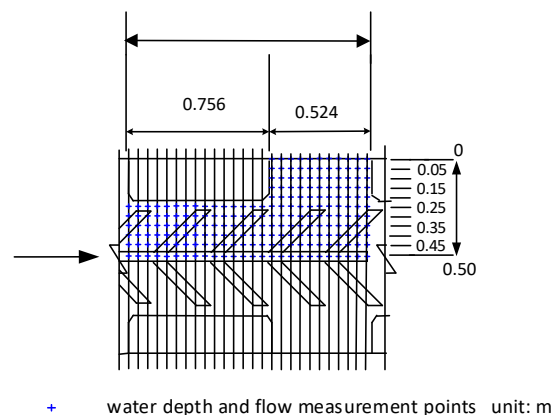


Figure 2. Flow measurements points.

3. Numerical Model

3.1. FLOW-3D

FLOW-3D is an advanced commercial CFD package based on the FVM that solves the Reynolds averaged Navier-Stokes equations (continuity and momentum) in the form shown below (Flow Science 2012).

Continuity equation:

$$\frac{V_F}{\rho c^2} \frac{1}{\partial t} + \frac{\partial}{\partial x}(\rho u A_x) + \frac{\partial}{\partial y}(\rho v A_y) + \frac{\partial}{\partial z}(\rho w A_z) = 0 \quad (1)$$

Momentum equations:

$$\frac{\partial u}{\partial t} + \frac{1}{V_F} \left\{ u A_x \frac{\partial u}{\partial x} + v A_y \frac{\partial u}{\partial y} + w A_z \frac{\partial u}{\partial z} \right\} = -\frac{1}{\rho} \frac{\partial p}{\partial x} + G_x + F_x \quad (2)$$

$$\frac{\partial v}{\partial t} + \frac{1}{V_F} \left\{ u A_x \frac{\partial v}{\partial x} + v A_y \frac{\partial v}{\partial y} + w A_z \frac{\partial v}{\partial z} \right\} = -\frac{1}{\rho} \frac{\partial p}{\partial y} + G_y + F_y \quad (3)$$

$$\frac{\partial w}{\partial t} + \frac{1}{V_F} \left\{ u A_x \frac{\partial w}{\partial x} + v A_y \frac{\partial w}{\partial y} + w A_z \frac{\partial w}{\partial z} \right\} = -\frac{1}{\rho} \frac{\partial p}{\partial z} + G_z + F_z \quad (4)$$

where V_F is the cell fractional volume (also used in Fractional Area/Volume Obstacle Representation (FAVOR)), ρ is fluid density, c is speed of sound, u, v, w are fluid velocity components in x, y, z directions, A_x, A_y, A_z fluid fractional area in x, y, z directions and FAVOR, p is pressure, G_x, G_y, G_z are gravitational components in x, y, z directions, and f_x, f_y, f_z are viscous accelerations in x, y, z directions.

It employs the volume of fluid (VOF) methods, which are based on the Eulerian approach to help it accurately define the boundary at the free surface (Hirt and Nichols 1981) and has a powerful capability to deal with free surface flows. FAVOR is applied to model complex geometries (Hirt and Sicilian 1985), making the code more versatile to most CFD applications. In addition, FAVOR was used to generate a good quality mesh, which contained 3 million cells, with edge lengths of 0.02 in all directions ($x, y,$ and z).

The code has 6 turbulence models: Prandtl mixing length model, the one-equation, the two-equation $k - \varepsilon$, RNG, $k - \omega$ models, and a Large Eddy Simulation (LES) model. In this paper we applied the LES turbulent closure model to allow comparison with the meshless approach. LES is able to provide an almost complete description of the instantaneous unsteady 3D turbulent flow field, resolving large-scale unsteadiness and asymmetries (large eddies) resulting from flow instabilities (Stoesser et al. 2009) by an eddy viscosity proportional a length scale multiplied by a measure of velocity fluctuations in the respective length scale (Eq. (5)) based on the work of Smagorinsky (1963). In addition, a vast number of studies in the last decade has shown LES to reproduce well the hydraulics of flow around structures (Palau-Salvador et al. 2008; Wang et al. 2016).

$$L = \delta x \delta y \delta z^{1/3} \quad (5)$$

In Eq. (5), velocity fluctuations are scaled by L magnitude by the average shear stress. These are then joined to a LES kinematic eddy viscosity as shown in the equation below (Flow Science 2012).

$$v_T = (cL)^2 \cdot \sqrt{2e_{ij}2e_{ij}} \quad (6)$$

The constant c ranges between 0.1 and 0.2 and e_{ij} is the strain tensor component.

3.2. XFlow

XFlow is another powerful CFD code that uses a proprietary, particle based, fully Lagrangian approach, which can easily handle traditionally complex problems (XFlow™ 2016). This therefore eliminates the need of a fluid domain meshing and in addition, surface complexity is not a limiting factor. The code features a novel particle based kinetic

algorithm that resolves the Lattice Boltzmann Method (LBM), and the state of the art LES modelling with advanced non-equilibrium wall models. LBM models fluid flow by using a particle mesh approach where the particles reside at the nodes of a discrete lattice mesh. The lattice Boltzmann equation may be written as (Luo et al. 2010):

$$f_i(x + c_i\Delta t, t + \Delta t) = f_i(x, t) + \Omega_i^B(f_1, \dots, f_b) \quad (7)$$

where f_i is particle distribution function in the direction i , c_i is discrete velocity in the direction i , Δt is time step, and $\Omega_i^B(f_1, \dots, f_b)$ is the Collision operator in central moment space.

As aforementioned, a lattice is generated in the computational grid and its resolution is adjusted through a resolved scale function. Two refinements algorithms may be used to better adapt the lattice to fit the requirements of the simulation: refinement near static walls and adaptive refinement. In this study, both refinement algorithms were disabled to maintain the same resolution with FLOW-3D. Resolved scale was fixed at 0.02 m throughout the computational domain.

Turbulence was modelled using the LES method, and sub-grid scales were modelled using the Wall-Adapting Local Eddy (WALE) summarized below (XFlow™ 2016):

$$v_{turbulent} = \Delta^2 \frac{(G_{\alpha\beta}^d G_{\alpha\beta}^d)^{3/2}}{(S_{\alpha\beta}^d S_{\alpha\beta}^d)^{5/2} + (G_{\alpha\beta}^d G_{\alpha\beta}^d)^{5/4}}, \quad (8)$$

where

$$S_{\alpha\beta} = \frac{1}{2} \left(\frac{\partial v_\alpha}{\partial r_\beta} + \frac{\partial v_\beta}{\partial r_\alpha} \right), \quad (9)$$

$$G_{\alpha\beta} = \frac{1}{2} (g_{\alpha\beta}^2 + g_{\beta\alpha}^2) - \frac{1}{3} \delta_{\alpha\beta} g_\gamma^2, \quad (10)$$

$$g_{\alpha\beta} = \frac{\partial v_\alpha}{\partial r_\beta}, \quad (11)$$

$$\Delta = C_w Vol^{1/3} \quad (12)$$

The WALE coefficient, (C_w) was not modified from the default of 0.2.

3.3. Boundary Conditions

For FLOW-3D, two fixed discharge levels (0.016 and 0.075 m³/s) were prescribed at the inlet boundary, while at the top and outlet, pressure was assigned. At the remaining surfaces, a wall boundary with a no-slip was activated. The computational domain was initialised by a 0.1 m flow depth. Similar boundary conditions were applied for XFlow, except at the inlet boundary. Instead, equivalent flow velocities were assigned for XFlow. These were obtained from the FLOW-3D code, which translated the discharge applied at the inlets to velocity. Summary of additional setup and computational times are shown in

Table 1 below.

Table 1. Summary of numerical models setup.

Parameter	FLOW-3D	XFlow
Mesh	3D structured	Meshless
Mesh resolution	0.02	0.02
Multiphase	VOF	Particle based tracking
Turbulence closure	LES	LES
Advection scheme	Explicit	Explicit
Courant number	0.7	0.7
Time step	Automatically controlled	Automatically controlled
Computational times (average)	9 hrs	7 hrs

4. Results and Discussion

Comparative studies of the models were conducted in the 3 regions of the fishway shown in Figure 1. Prior to in-depth analysis, the models were validated by comparing observed and simulated flow depths. Both models (FLOW-3D and XFlow) managed to produce physically consistent flow depth, with accuracies of up to 99 % and 89 % for FLOW-3D and XFlow (at 0.016 m³/s), respectively. At 0.075 m³/s, the model's performance was almost similar, although FLOW-3D was still better (Table 2). Moreover, XFlow poorly estimated flow depth as flow covered the fish-bone area, while FLOW-3D captured this variation well.

Table 2. Comparison of observed and simulated flow depths.

Location	0.016 m ³ /s flow depth (m)			0.075 m ³ /s flow depth (m)		
	Observed	FLOW-3D	XFlow	Observed	FLOW-3D	XFlow
Channel Area	0.092	0.102	0.11	0.200	0.193	0.21
Rest area A	0.055	0.064	0.08	0.16	0.143	0.15
Rest area B	0.071	0.081	0.084	0.187	0.172	0.20
R²		0.997	0.899		0.988	0.972

4.1. Flow Structure and Velocity

Figure 3 compares flow structure using stream flows predicated in FLOW-3D and XFlow during the simulation. The flow structure is better predicted by the FLOW-3D than by XFlow when compared to actual observations (Figure 4). Swirling flow is well captured behind the blocks (area A) in FLOW-3D, while in XFlow, this is only visible towards the end of the channel. This may be attributed to the resolution of the lattice mesh. Area B shows less turbulence as observed in the laboratory experiments. In this study an attempt was made to maintain similar resolution for both models in order to enforce comparison. Further refinement of the XFlow code to 0.01 significantly improved the flow structure (results not shown); however, computational time was tripled to 4 days. With the original setup, XFlow was able to complete the simulation in less than 7 hours, while FLOW-3D completed the simulation in 9 hours in an i7-7700K, 4.2GHz and 64 GB of installed memory.

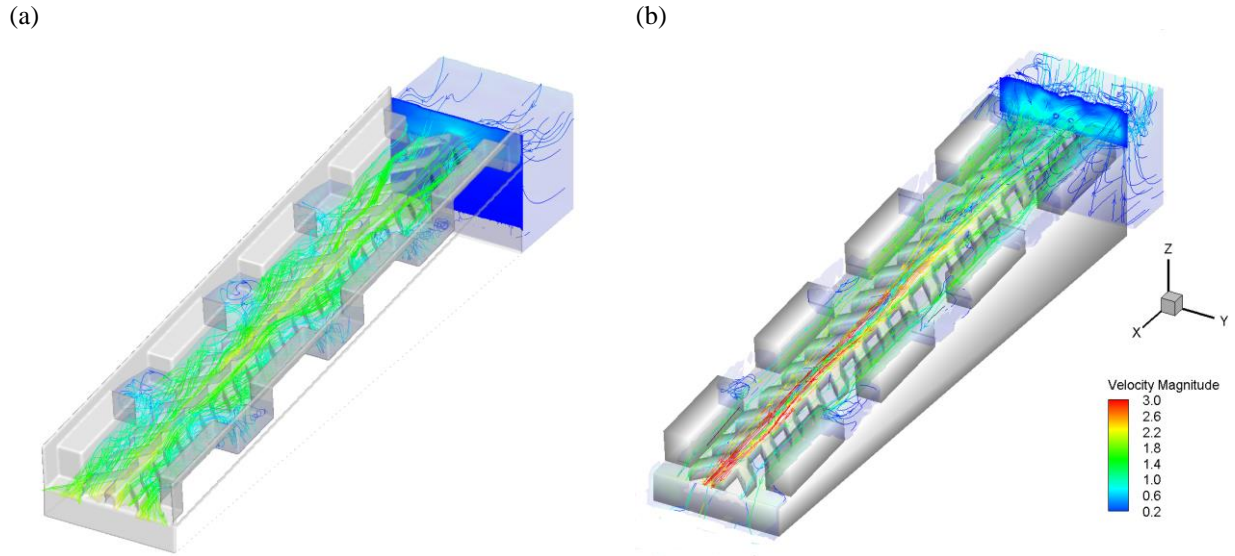


Figure 3. Stream traces for (a) FLOW-3D and (b) XFlow at $0.075 \text{ m}^3/\text{s}$.

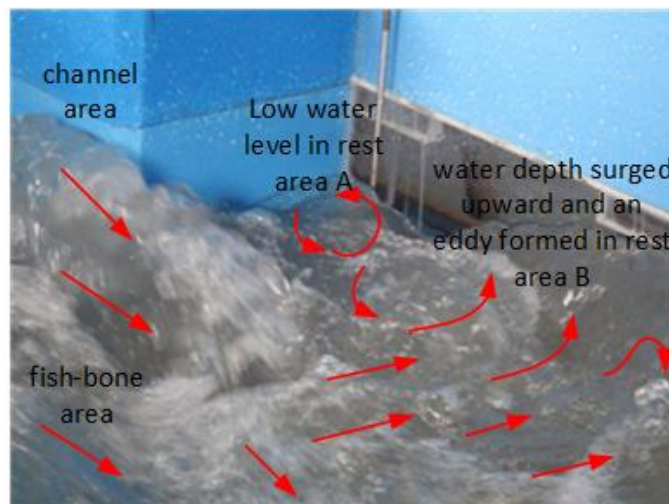


Figure 4. Flow fields in the different regions of the fishway.

Flow variation and velocity is qualitatively better captured in FLOW-3D than in XFlow (Figure 5 and Figure 6). Flow covered the fish-bone areas in the laboratory experiment (Figure 5a), a similar pattern shown by FLOW-3D (Figure 5b). Where flow is confined, both models performed reasonably well considering the refinement resolution applied, especially for XFlow, which clearly required higher resolution for the cases applied herein. XFlow was further less accurate in capturing the flow patterns along fish-bone areas, as it indicated flow patterns that resembled a discharge of $0.075 \text{ m}^3/\text{s}$ shown in Figure 6. This may be due to the inlet boundary condition applied in XFlow. The code allows velocity inlet, while in FLOW-3D, we were able to apply the discharge as it was during the laboratory experiment.

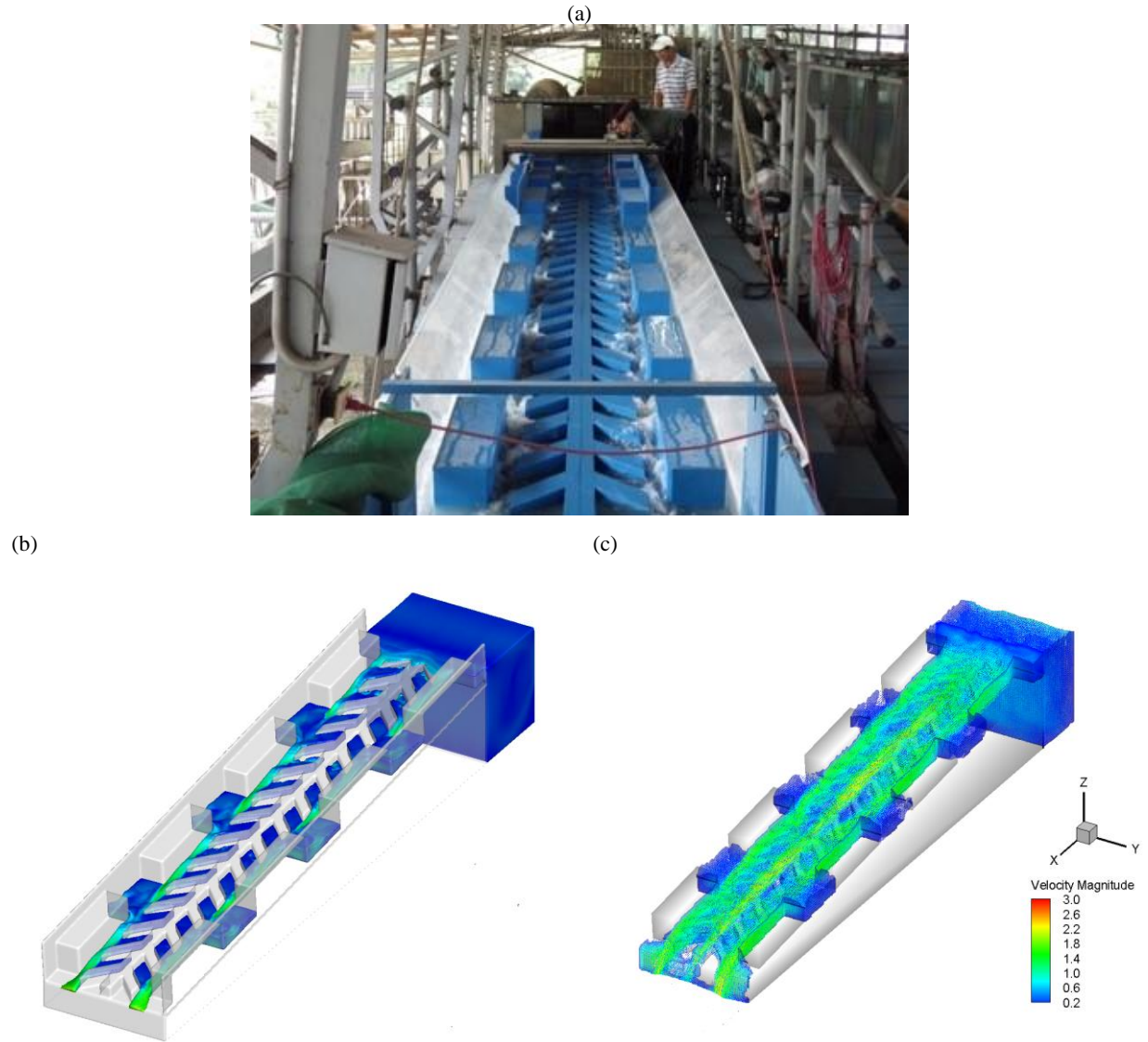


Figure 5. Flow pattern variation and velocity magnitude at a discharge of $0.016 \text{ m}^3/\text{s}$ at (a) laboratory, (b) FLOW-3D, and (c) XFlow.

Unlike with the case of low discharge, $0.016 \text{ m}^3/\text{s}$, both models showed little variation in the velocity magnitude and flow patterns. Water covered the fish-bone areas, and velocity was strongest along this area, followed by the channel areas and finally the rest areas. As illustrated in the laboratory, flow velocity along the channel areas (confined region between fish-bones and blocks) was relatively higher at $0.016 \text{ m}^3/\text{s}$ and was comparable to velocity at the fish-bone areas under $0.075 \text{ m}^3/\text{s}$ as shown by both Figure 5 and Figure 6.

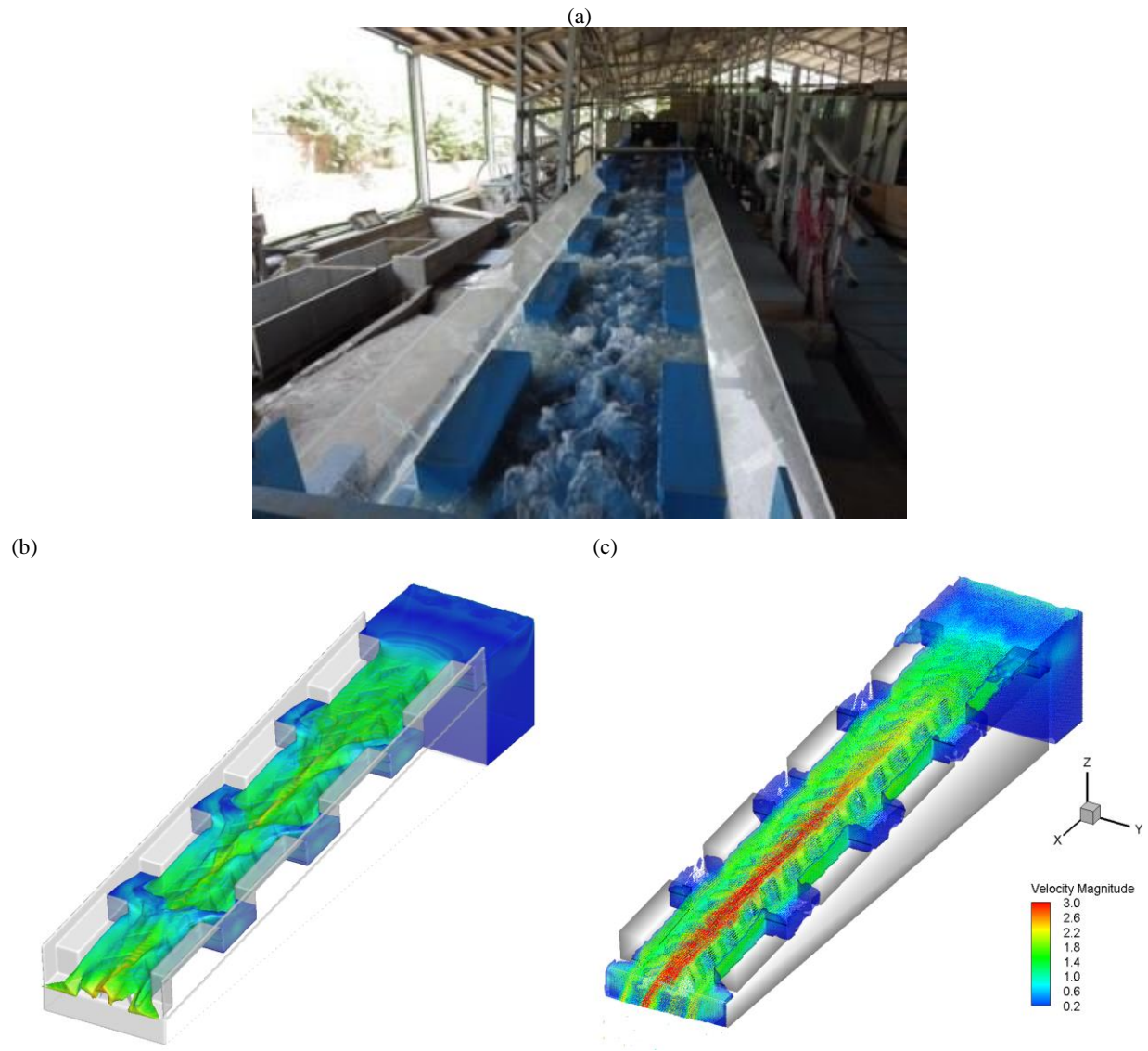


Figure 6. Flow pattern variation and velocity magnitude at a discharge of $0.075 \text{ m}^3/\text{s}$ at (a) laboratory, (b) FLOW-3D, and (c) XFlow.

Figure 7 compares velocity components, u (longitudinal), v (lateral), and w (vertical), predicted in FLOW-3D and XFlow at 200 sampling points along the fish-bone area (refer to Fig. 1). Due to space limitations, we present the components at this region, excluding channel and rest areas. For u , a general agreement ($R^2 = 0.49$) is observed between these models in the longitudinal direction, indicating strong agreement. On the contrary, there is no agreement for v and w , indicating major differences in the flow structure in both lateral and vertical directions (0.003 and 0.002, respectively). The differences are believed to be due to the turbulent closures, i.e. the formulations of the LES in both codes. In depth investigations are needed to explore the disagreement displayed by these models. Based on the findings of Chen et al. (2017), both models could better explain the migration of Eels, since they utilized mostly the fishbone areas to migrate upstream. Lateral movements would have to be validated by experimental studies. Nonetheless, FLOW-3D seems to have captured lateral movements of water well, as illustrated by Fig. 6 above.

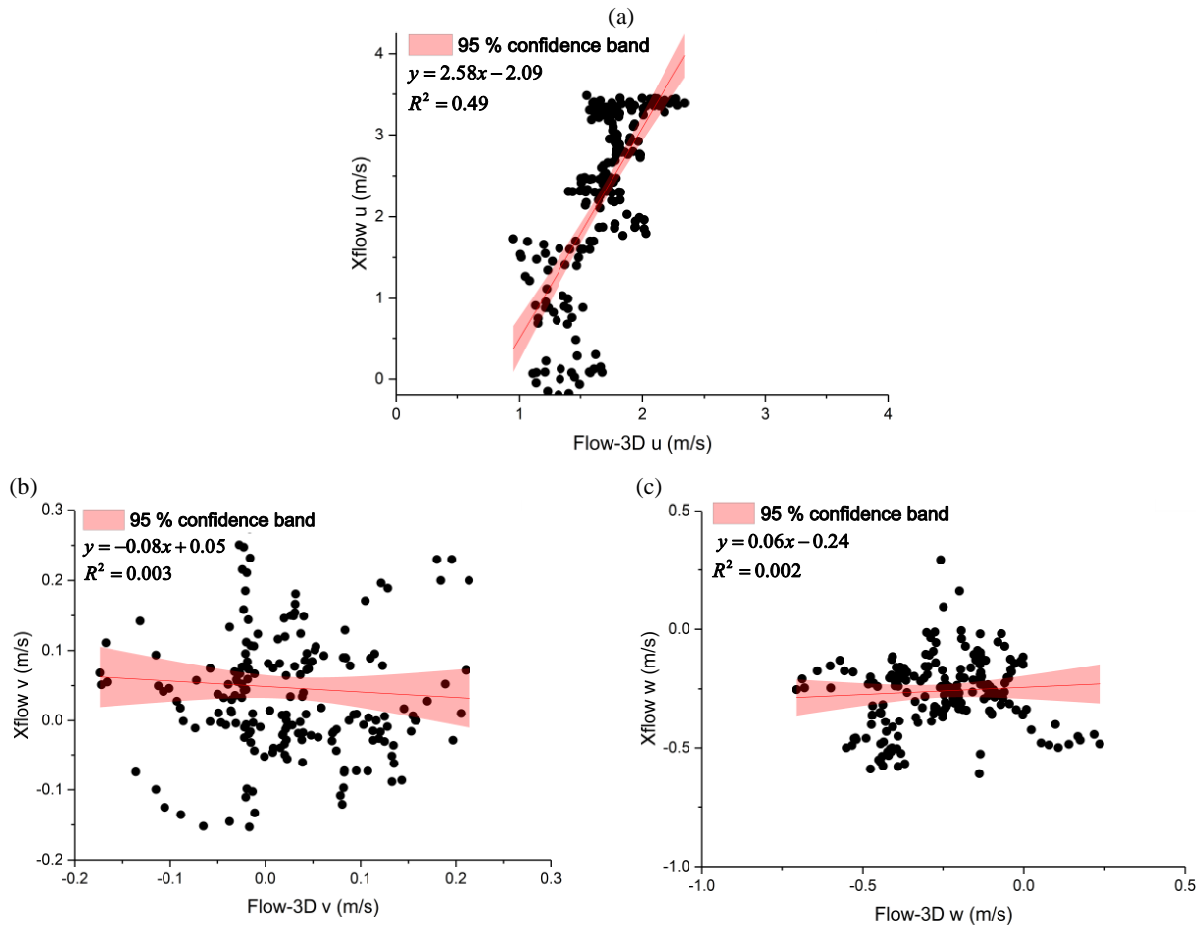


Figure 7. Scatter plot of velocity components with (a) u direction, (b) v direction, and (c) w direction.

5. Conclusion

Selecting the most applicable numerical code among the currently available models can be a daunting task. In this qualitative assessment of mesh-based and meshless models, FLOW-3D appears to better reproduce the flow patterns and flow structure in the fish-bone-type fishways. There was, however, an additional computation cost of approximately 2 hrs. XFlow on the other hand presented a better alternative to FLOW-3D especially when general assessment is sought. Both codes agreed on the u -direction, while no agreement was observed at both lateral and vertical flow structure. The meshless code seemed to have performed better at the discharge of $0.075 \text{ m}^3/\text{s}$ than at the lower discharge. Additional tweaks and refinement of lattices in XFlow seem to be necessary to attain high accuracies. The comparison made in this study presents a base to an in-depth assessment of these codes, which is in the works at the time of the qualitative assessment. Finally, we observed that meshless codes significantly reduced the model setup time, as the main parameter related to the lattice was the refinement algorithm.

6. References

- Bayon, A., Valero, D., García-Bartual, R., Vallés-Morán, F.J., and López-Jiménez, P.A. (2016). "Performance assessment of OpenFOAM and FLOW-3D in the numerical modeling of a low Reynolds number hydraulic jump." *Environ. Model. Software*, 80, 322-335.
- Chen, F., Xu, A.G., Zhang, G.C., and Li, Y.J. (2010). "Three-Dimensional Lattice Boltzmann Model for High-Speed Compressible Flows." *Communications in Theoretical Physics*, 54(6), 1121.
- Chen, S.C., Wang, S.C., and Tfwala, S.S. (2017). "Hydraulics driven upstream migration of taiwanese indigenous fishes in a fish-bone-type fishway." *Ecol. Eng.*, 108(Part A), 179-193.
- Flow Science (2012). *Flow-3D User Manual: v10.1*, Flow Science, Inc.
- Harlow, F.H. (1964). "The Particle-in-Cell Computing Method for Fluid Dynamics." *Methods in Computational Physics*, 3, 319-343.
- Hirt, C.W., and Nichols, B.D. (1981). "Volume of fluid (VOF) method for the dynamics of free boundaries." *Journal of Computational Physics*, 39(1), 201-225.
- Hirt, C.W., and Sicilian, J.M. "A porosity technique for the definition of obstacles in rectangular cell meshes." *Proc., Proceeding 4th International Conference on Numerical Ship Hydrodynamics*.
- Kueh, T.C., Beh, S.L., Rilling, D., and Ooi, Y. (2014). "Numerical Analysis of Water Vortex Formation for the Water Vortex Power Plant." *International Journal of Innovation, Management and Technology*, 5(2), 111-115.
- Liu, J., Koshizuka, S., and Oka, Y. (2005). "A hybrid particle-mesh method for viscous, incompressible, multiphase flows." *Journal of Computational Physics*, 202(1), 65-93.
- Luo, L.S., Krafczyk, M., and Shyy, W. (2010). "Lattice Boltzmann Method for Computational Fluid Dynamics." *Encyclopedia of Aerospace Engineering*, John Wiley & Sons, Ltd.
- Markauskas, D., Kruggel-Emden, H., Sivanesapillai, R., and Steeb, H. (2017). "Comparative study on mesh-based and mesh-less coupled CFD-DEM methods to model particle-laden flow." *Powder Technology*, 305, 78-88.
- Palau-Salvador, G., Stoesser, T., and Rodi, W. (2008). "LES of the flow around two cylinders in tandem." *Journal of Fluids and Structures*, 24(8), 1304-1312.
- Prostomolotov, A.I., Iliasov, H.H., Verezub, N.A., and Vladimirova, N.A. (2014). "Application of XFlow code for numerical simulation of aero and hydrodynamic structures." *Fluxes and structures in Fluids: International Conferences* Saint Petersburg, Moscow, 170-177.
- Shakibaeinia, A., and Jin, Y.C. (2011). "A mesh-free particle model for simulation of mobile-bed dam break." *Adv. Water Resour.*, 34(6), 794-807.
- Smagorinsky, J. (1963). "General circulation experiments with the primitive equations." *Monthly Weather Review*, 91(3), 99-164.
- Stoesser, T., Salvador, G.P., Rodi, W., and Diplas, P. (2009). "Large Eddy Simulation of turbulent flow through submerged vegetation." *Transport in Porous Media*, 78(3), 347-365.
- Wang, Y., Wang, L., Zhu, H., Tang, H., and Wei, G. (2016). "A Numerical Study of the Forces on Two Tandem Cylinders Exerted by Internal Solitary Waves." *Mathematical Problems in Engineering*, 2016, 15.
- XFlow™ (2016). "User guide." DS Simulia.